# Influence of ion energy and substrate temperature on the optical and electronic properties of tetrahedral amorphous carbon (*ta*-C) films

M. Chhowalla[a)]
*University of Liverpool, Department of Electrical Engineering and Electronics, Liverpool L69 3BX, United Kingdom*

J. Robertson and C. W. Chen
*University of Cambridge, Department of Engineering, Trumpington Street, Cambridge CB2 1PZ, United Kingdom*

S. R. P. Silva
*University of Surrey, Department of Electronics and Electrical Engineering Guildford, Surrey GU2 5XH, United Kingdom*

C. A. Davis
*Plasma Research Laboratory, Research School of Physical Sciences and Engineering, Australian National University, Canberra ACT 2601, Australia*

G. A. J. Amaratunga
*University of Liverpool, Department of Electrical Engineering and Electronics, Liverpool L69 3BX, United Kingdom*

W. I. Milne
*University of Cambridge, Department of Engineering, Trumpington Street, Cambridge CB2 1PZ, United Kingdom*

(Received 18 March 1996; accepted for publication 23 September 1996)

The properties of amorphous carbon (*a*-C) deposited using a filtered cathodic vacuum arc as a function of the ion energy and substrate temperature are reported. The $sp^3$ fraction was found to strongly depend on the ion energy, giving a highly $sp^3$ bonded *a*-C denoted as tetrahedral amorphous carbon (*ta*-C) at ion energies around 100 eV. The optical band gap was found to follow similar trends to other diamondlike carbon films, varying almost linearly with $sp^2$ fraction. The dependence of the electronic properties are discussed in terms of models of the electronic structure of *a*-C. The structure of ta-C was also strongly dependent on the deposition temperature, changing sharply to $sp^2$ above a transition temperature, $T_1$, of $\approx$200 °C. Furthermore, $T_1$ was found to decrease with increasing ion energy. Most film properties, such as compressive stress and plasmon energy, were correlated to the $sp^3$ fraction. However, the optical and electrical properties were found to undergo a more gradual transition with the deposition temperature which we attribute to the medium range order of $sp^2$ sites. We attribute the variation in film properties with the deposition temperature to diffusion of interstitials to the surface above $T_1$ due to thermal activation, leading to the relaxation of density in context of a growth model. © *1997 American Institute of Physics.* [S0021-8979(97)01101-8]

## I. INTRODUCTION

There is currently a great deal of interest in the deposition of amorphous carbon films containing a sizable fraction of $sp^3$ bonds. This so-called diamondlike carbon (DLC) has a number of technologically valuable features such as high hardness, low friction coefficient, chemical inertness, and low electron affinity.[1] It is now well established that tetrahedral $sp^3$ bonding is promoted by deposition from medium energy carbon ions.[2] A highly tetrahedral form of amorphous carbon, referred to as *ta*-C, containing up to 85% $sp^3$ has been prepared using filtered beams of carbon ions. The filtering removes particulates and neutrals and provides a relatively monoenergetic beam of singly charged ion species. Several techniques such as mass selected ion beam (MSIB),[3,4] laser ablation of graphite,[5–8] and filtered cathodic vacuum are (FCVA)[9–15] have been used to deposit *ta*-C. An industrial or laboratory scale FCVA is particularly useful for depositing *ta*-C because it provides a highly ionized plasma and high deposition rates of up to 3 nm $s^{-1}$.[8–15]

The bonding of *ta*-C deposited at room temperature has been extensively studied. The density, $sp^3$ fraction, compressive stress, and resistivity were found to depend strongly on the ion energy and pass through a maximum at ion energies ranging from 50 to 240 eV.[10] The present paper extends the work in two directions. First, we describe the electronic and optical properties of FCVA deposited *a*-C as a function of the ion energy and relate them to models of electronic structure.[16–19] We also report on the effect of deposition temperature on the structural characteristics of FCVA deposited *a*-C films with particular reference to the optical and electronic properties. Related studies have been carried out on *a*-C prepared by other methods.[15,20–22] A sharp transition from *ta*-C to $sp^2$ bonded *a*-C was observed for films deposited above the transition temperature while the variation in

a)Electronic mail: muc@liv.ac.uk

the electronic and optical properties was more gradual with the deposition temperature. We place these results on the bulk electronic and optical properties in the context of changes in carbon bonding structure within the films. Furthermore, the transition temperature was found to decrease with ion energy. The transition is used to understand further details of the film growth mechanism known as subplantation.[3,4,23] In subplantation, incident ions with sufficient energy penetrate the atomic surface layer generating $sp^3$ bonding. However, ions with excess energy migrate to the surface decreasing the density to that of $sp^2$ bonded carbon.

## II. EXPERIMENTAL DETAILS

The $a$-C films were deposited using a FCVA system where the carbon plasma is obtained from a graphite cathode of 99.999% purity. The arc is initiated by contacting the cathode with a retractable graphite anode of similar purity. The carbon plasma is then transported around a 90° curved magnetic solenoid filter to remove neutrals and particulates also generated by the arc.[24] The solenoid, in our case, produces an axial magnetic field of ≈25 mT which guides the electrons around the bend creating an electrostatic potential which causes the ions to follow the same curve. Therefore, unlike the MSIB, the FCVA does not provide ion mass or charge selection. A base pressure of $10^{-5}$ Pa was achieved using two diffusion pumps which rose to $10^{-3}$ Pa during deposition.

The $a$-C films were deposited on $n$-type (001) silicon substrates clamped to a copper block. The incident energy of the carbon ions was varied by applying a dc voltage to the copper block. The total ion energy is therefore the sum of the incident ion energy and the applied voltage. The ion energy was measured at the substrate position using a retarding field energy analyzer with a Faraday cup.[25] The temperature of the substrate was varied over 20–500 °C by a heater attached to the back of the copper block. Depositions below room temperature (RT) were carried out by cryogenically cooling the substrate holder. The temperature was measured by a thermocouple attached behind the silicon substrate. For depositions above RT, all samples were heated to 500 °C initially and cooled to the deposition temperature where they were held for 10–15 min before initiating the plasma.

The stress in the films was derived by measuring the radius of curvature of the substrate before and after deposition and applying Stoney's equation.[26] Films for optical and electronic measurements were deposited on quartz substrates. The incident ion energy for this case was varied by applying rf voltage. The optical properties were determined from the reflectance and transmittance data using a double beam spectrometer in the 200–900 nm wavelength range. The electrical conductivity of the films was measured by evaporating 5 mm×0.5 mm Al electrode gap cells onto $a$-C. The surface roughness was determined using atomic force microscopy (AFM) where the area roughness $R_a$ is defined as

$$R_a = \Sigma \frac{|Z_i - Z_{\text{ave}}|}{N}, \tag{1}$$

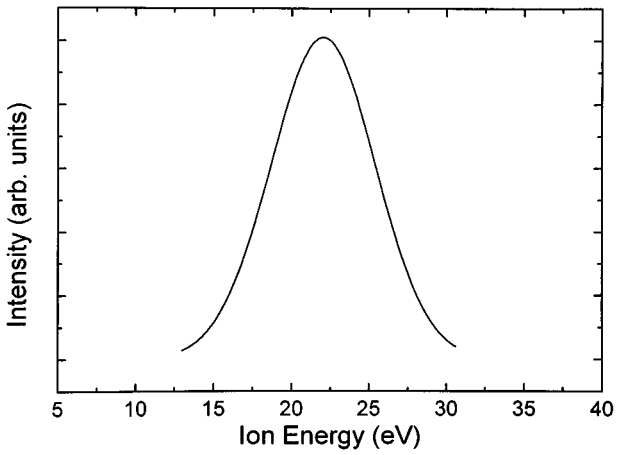


FIG. 1. Ion energy distribution (IED) of the filtered plasma beam at a magnetic field strength of 25 mT. The full width at half-maximum of the distribution was found to be 7–9 eV. The ion energy did not vary significantly with the magnetic field strength.

where $N$ is the number of height measurements, $Z_i$ is the current surface height, and $Z_{\text{ave}}$ is the average height within the given area.

The bonding in $a$-C was determined by electron energy loss spectroscopy (EELS)[10] using a Philips CM30 transmission electron microscope (TEM) fitted with a Gatan 666 EEL spectrometer. The films were prepared for EELS by dissolving the silicon substrate in a dilute $HF+HNO_3$ solution and placing the freed film onto copper support grids. The TEM was operated at 100 kV and the EELS collection angle was 10 mrad. The fraction of $sp^3$ bonding was derived from the carbon $K$ edge, which consists of a peak at 285 eV due to $1s-\pi^*$ transitions from the $sp^2$ sites and a step at 289 eV due to excitations into the $\sigma^*$ states. The $sp^2$ fraction is given by the ratio of the 285 eV peak to 289 eV step, normalized to their ratio in graphitic carbon, which contains 100% $sp^2$ bonding. The microscopic density of each film can be derived from the plasmon energy in the low energy EEL spectrum.[10]

## III. RESULTS

### A. Ion beam characteristics

The 90° magnetic solenoid filter guides the plasma around the bend, filters out the particulates and neutrals, and also focuses the plasma. The ion energy distribution (IED) of the carbon plasma at the exit of the magnetic filter is shown in Fig. 1. The initial ion energy was found to be ≈21 eV and did not vary significantly with the filter current. The high initial ion energy is attributed to a ''potential hump'' arising above the cathode spot.[27] The IED is clearly seen to be Gaussian in shape and not Maxwellian as previously proposed.[28] The full width at half-maximum (FWHM) of the IED was found to be 7–9 eV. The large FWHM is attributed to multiply charged species which may be present in the plasma.[28]

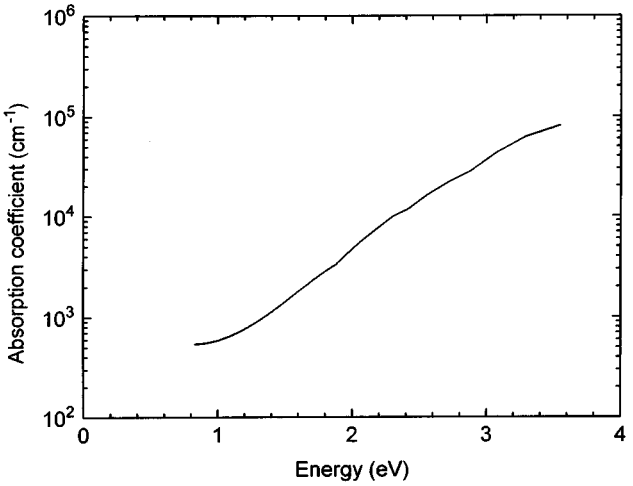


FIG. 2. Absorption coefficient vs the photon energy. The plot is a combination of measurements using photothermal deflection spectroscopy (PDS) and an UV spectrometer.

### B. Properties of films deposited at ambient temperature

The optical absorption spectrum of *ta*-C deposited at ambient temperature on quartz at an ion energy of 90 eV is illustrated in Fig. 2. The plot is a combination of data from reflection-transmission and photothermal deflection spectroscopy (PDS) measurements. The optical gap of an amorphous semiconductor is conventionally defined as either the energy ($E_{04}$) at which the absorption coefficient, $\alpha$, $=10^4$ cm$^{-1}$ or as the Tauc gap, $E_g$, found by fitting $\alpha$ to: $\alpha E = B(E-E_g)^2$, where $E$ is the photon energy ($h\nu$) and $B$ is an empirical constant. The variation of the $sp^3$ fraction, $E_{04}$ Tauc gap, refractive index, and resistivity as a function of the ion energy at ambient temperature is shown in Fig. 3. The $sp^3$ fraction, optical gap, and refractive index are seen to reach a maximum at an ion energy of ≈90 eV, indicating there is a strong correlation among the properties. In Fig. 4, it can be seen that the optical gap of *ta*-C, although lower than for the hydrogenated films, varies in a similar fashion with the $sp^2$ fraction to other forms of *a*-C:H[29,30] and *ta*-C:H,[31] indicating that the gap primarily depends on the $sp^2$ sites and only weakly on the hydrogen content.

The dependence of the optical gap on the $sp^2$ fraction may be expected from the electronic structure of *a*-C since the band gap is determined by the $\pi$ states of the $sp^2$ sites,[16] as these states lie closest to the Fermi level ($E_F$). Therefore, the fraction and arrangement of the $sp^2$ sites are important in influencing the optical and electronic properties of the films. It has been proposed[16] that the $sp^2$ sites pair up to form $\pi$ bonds and segregate into clusters within the $sp^3$ matrix. The formation of the clusters is opposed by disorder in the film.[17] If the disorder is low, the width of the $\pi$ band depends on the cluster size such that the optical gap varies inversely to the cluster size.[18] However, it is now believed that any $sp^2$ clusters are relatively small,[17] indicating the band gap depends on both cluster size and local distortions of the $\pi$ bonding and that no simple relationship for the band gap exists.

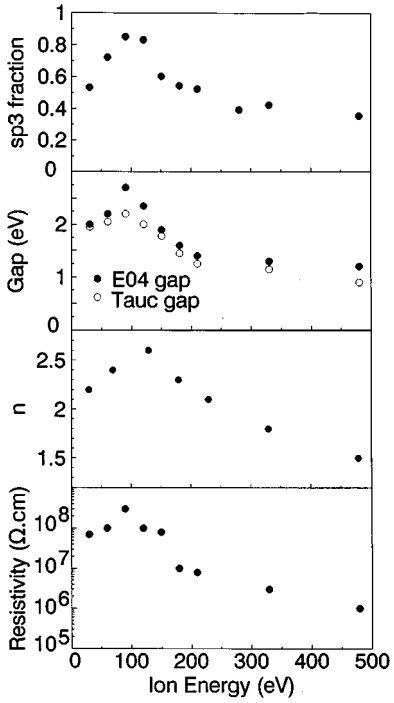


FIG. 3. Graphs of (a) $sp^3$ fraction, (b) Tauc, $E_{04}$ optical band gaps, (c) refractive index, and (d) resistivity vs the ion energy. All properties are correlated to each other. The optical gap and the resistivity values are seen to drop sharply at higher ion energies.

The gradual change in the band gap with the $sp^2$ content in Fig. 4 suggests that the $\pi$ bands become narrower and the $\pi$–$\pi^*$ gap widens as $sp^2$ fraction decreases. The importance of $\pi$ bonding is indicated by the steady increase in the $E_g$ even when 20% $sp^2$ sites remain in *ta*-C. The similar variation of the gap in *a*-C:H and *ta*-C (from Fig. 4) is particularly important at low $sp^2$ contents where the $sp^2$ sites are embedded in a rigid matrix in *ta*-C but a rather floppy matrix in polymeric *a*-C:H. This suggests that the gap and the $\pi$ bonding of the $sp^2$ sites depend primarily on the $sp^2$ fraction and much less on the nature of the surrounding matrix or the hydrogen content, as originally thought.[16]

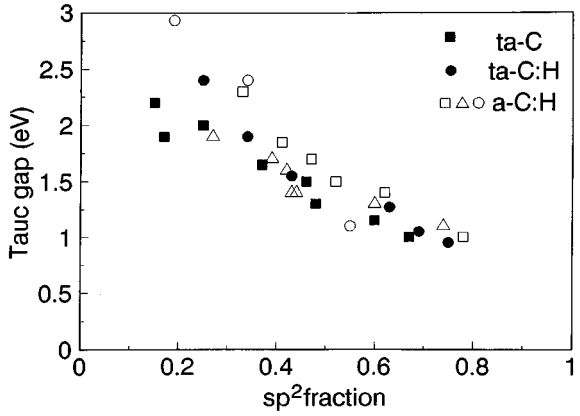


FIG. 4. Optical band gap vs the $sp^2$ fraction of *ta*-C and different types of hydrogenated *a*-C films for comparison. The gap is found to decrease linearly with the $sp^2$ fraction.

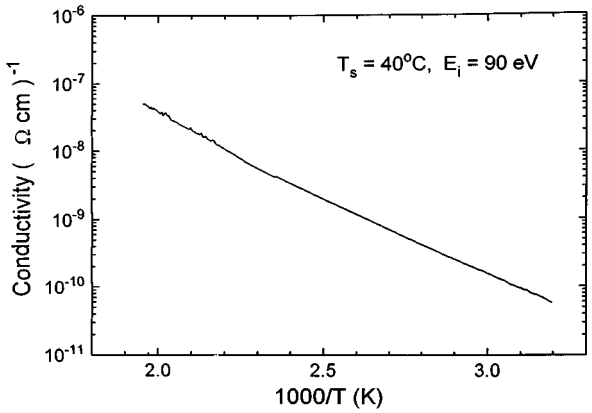


FIG. 5. Plot of conductivity vs the temperature. Note the trend is a straight line, in contrast to hydrogenated *a*-C which is curved.

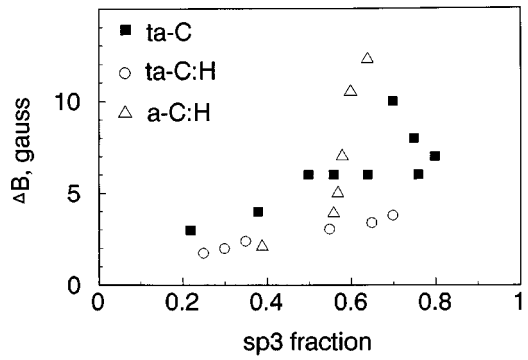


FIG. 6. Linewidth of the ESR signal vs the $sp^3$ fraction. Note the unhydrogenated *a*-C follows a similar trend to its hydrogenated counterparts.

The absorption edge for *ta*-C is (from Fig. 2) observed to be much broader than in other semiconductors such as *a*-Si:H,[32] indicating a high degree of disorder in the film. The lower part of the absorption edge in Fig. 2 follows only an approximate exponential dependence required for the Urbach tail. Nevertheless, the Urbach slope, determined by drawing a tangent to the log of the absorption coefficient at $\alpha=2\times10^3$ cm$^{-1}$ in Fig. 2, is found to be 300 meV which similar to *a*-C:H[1] and *ta*-C:H[31] and compares to 55 meV for a high quality *a*-Si:H.[32]

The variation of the resistivity as a function of the ion energy at RT is plotted in Fig. 3(d). The sharp decrease in resistivity at higher ion energies is attributed to increase in disorder in the film due to energetic ion bombardment leading to a higher number of gap states. The electronic conductivity of *ta*-C as a function of inverse temperature is shown in Fig. 5. It should be noted that *ta*-C differs from hydrogenated *a*-C in which the Arrhenius plot is curved.[33] The activation energy ($\Delta E$) from Fig. 5 was found to be $\approx$0.45 eV, much less than half the band gap (2.3 eV), indicating the Fermi level lies away from the midgap. Measurements on *ta*-C/Si heterojunctions, nitrogen doping data, and recently fabricated thin film transistors suggest $E_f$ lies below midgap and that undoped *ta*-C is *p* type.[34–36] Furthermore, electronic calculations suggest $E_f$ is pinned below the midgap by defect sites.

The singly occupied defect states at $E_f$ give rise to an electronic spin resonance (ESR) signal. The defect density in *ta*-C as a function of the ion energy has been found to be very high,[37] approaching that of unhydrogenated *a*-Si. The spin density in principle is controlled by two factors, disorder and bonding. The large defect density observed in *ta*-C presumably arises due to ion induced disorder from the deposition process. However, this is countered by the energy gain in $\pi$ bonding which, according to calculations,[18] tends to reduce the defect densities at high $sp^3$ contents.

The ESR signal linewidth as a function of the $sp^2$ fraction is shown in Fig. 6. It is presently unclear if the defects in *ta*-C arise from single $sp^2$ sites or clusters. Information on the structure and chemistry for most materials can be derived from the ESR *g* factor, but this is less helpful in the case of *ta*-C because most defects lie at $g=2.0028$, similar to all other forms of carbon. Therefore the linewidth is the main source of information in *ta*-C. The linewidth can be attributed to disorder, dipolar broadening, exchange narrowing, or the presence of numerous subsidiary lines. Unlike *a*-Si:H, where the ESR line of dangling bonds is Gaussian due to the dominance of disorder broadening,[32] the *ta*-C line is a Lorentzian, eliminating disorder broadening as a factor. Also, the linewidth in *ta*-C was found not to vary with the microwave excitation frequency indicating the signal consists of a single line.[38] Additionally, dipolar broadening arises from interaction with hydrogen nuclei. Therefore, the absence of hydrogen makes the ESR data in *ta*-C very informative. The linewidth of *ta*-C in Fig. 6 is seen to vary in a similar fashion to other forms of *a*-C:H containing H, thus the linewidth is not due to dipolar broadening by H. Therefore, the linewidth is primarily attributed to exchange narrowing, also suggested by others.[39,40] The linewidth will then vary linearly with the localization of unpaired electron or inversely with the ''cluster'' size over which it is delocalized, accounting for the decrease in linewidth with the $sp^2$ fraction for all *a*-C(:H) seen in Fig. 6.

### C. Variation with deposition temperature

The variation of the $sp^3$ fraction, plasmon energy compressive stress, and surface roughness as a function of the substrate temperature ($T_s$) for 90 and 130 eV ions is shown in Fig. 7. Each property is found to be independent of $T_s$ initially but falls sharply at a transition temperature ($T_1$) of $\approx$200 and 140 °C for ion energies of 90 and 130 eV, respectively. Films appear to undergo a transition from *ta*-C to essentially $sp^2$ bonded *a*-C above $T_1$.

A similar trend was previously observed for *ta*-C deposited by MSIB,[20,21] laser initiated pulsed arc system[15] and also for *ta*-C:H deposited using a plasma beam source.[22] The $T_1$ ($\approx$140 °C) in the 130 eV case is equivalent to that observed for the MSIB system[20,21] but much lower than that observed for *ta*-C:H.[22] A similar decrease in the transition temperature with ion energy was found for *ta*-C:H while MSIB deposited films show an opposite trend. The reason for this discrepancy is presently unclear.

All films exhibited extremely smooth surfaces ($R_a\approx$0.2 nm) making them useful for high performance tribological applications. The roughness was found to remain constant

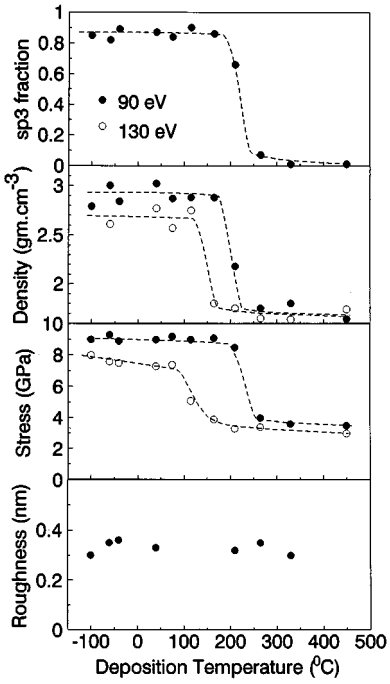


FIG. 7. Graphs of (a) $sp^3$ fraction, (b) plasmon energy, (c) compressive stress, and (d) surface roughness as a function of the substrate temperature at two ion energies. The sharp decrease in the properties correlates to a transition from *ta*-C to *a*-C. The transition temperature for the higher energy film is seen to decrease from ≈200 to 140 °C. Note the film roughness does not change with deposition temperature, in contrast to films deposited using MSIB (Ref. 37).

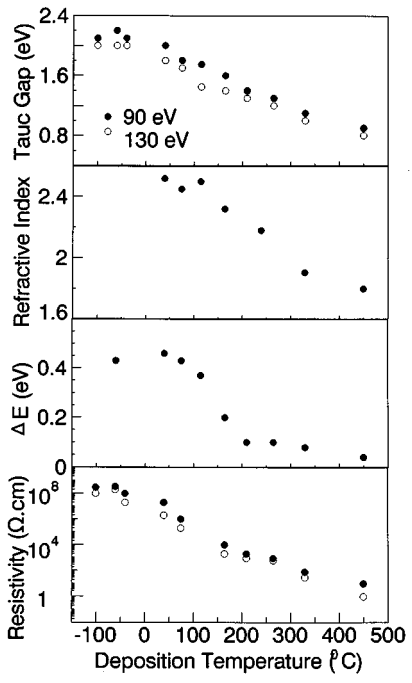


FIG. 8. Graphs of (a) Tauc gap, (b) refractive index, (c) activation energy, and (d) resistivity vs the substrate temperature. Note that the decline in these properties is more gradual than those plotted in Fig. 7.

with the deposition temperature, in contrast to the films deposited using MSIB.[20,21] The increase in surface roughness with $T_s$ in MSIB is attributed to the diffusion of shallowly implanted (subplanted) species to the surface. However, since the deposition rates are significantly higher in the FCVA case, we infer that the arrival rate of an ion is of the order of the diffusion rate.

The deposition rate was found to sharply increase at $T_1$, which is correlated to the drop in the plasmon energy (film density) with $T_s$. We attribute the increase in growth rate to the predominance of the low density $sp^2$ phase above $T_1$ leading to an increase in film thickness. The *a*-C films deposited above $T_1$ were also examined using a TEM and were found to possess the (0002) interlayer diffraction peak characteristic of microcrystalline graphite suggesting that a phase transition has occurred. However, the phase transition cannot be regarded in classical thermodynamic terms since it is not reversible. Furthermore, the presence of microcrystalline graphite suggests the film has somehow experienced very high local temperature during deposition.

The variation of optical gap, refractive index, activation energy, and resistivity with $T_s$ of films deposited on quartz is plotted in Fig. 8. The properties are well correlated to each other and decline gradually with $T_s$, in contrast to the sharper drop in $sp^3$ fraction, compressive stress, and plasmon energy. The possibility that the contrasting trends could arise from the difference in the thermal conductivity of quartz and silicon was checked by measuring the refractive index of the films on silicon by ellipsometry. The trend was found to be similar to the optical gap as seen in Fig. 8(b), suggesting that the difference in variation between the $sp^3$ fraction and the optical and electronic properties is real. The gap and resistivity are observed to continue rising with decreasing $T_s$ below room temperature. The gradual change in the optical and electrical properties well below $T_1$ suggests that although the $sp^2$ content is low in the most diamondlike films, the optical and electronic properties are nevertheless controlled by the residual $sp^2$ fraction. Therefore, there is no ''critical'' $sp^2$ fraction at which sudden changes in the optical and electronic properties occur. Furthermore, the fall of the gap and resistivity with increasing temperature below $T_1$ suggests that the $sp^2$ sites begin to show increasing order well below the transition temperature.

The resistivity and conductivity activation energy ($\Delta E$) also fall gradually with increasing substrate temperature as shown in Figs. 8(c) and 8(d), consistent with the change in the band gap. Again, the resistivity is seen to increase further for deposition below room temperature. The $\Delta E$ is observed to be less than half the optical gap because $E_f$ lies below midgap, as previously noted.

## IV. DEPOSITION MECHANISM

The formation of *ta*-C is generally described by the subplantation model[3,4,10,23,41] which is based on incident energetic ions penetrating the surface and providing subsurface growth. The decline in density at higher ion energies is attributed to implanted ions diffusing back to the surface, either by thermally activated diffusion during a thermal spike stage of thermal dissipation after the cascade[23,42] or due to defect formation by radiation damage during cascade.[3,4,43] The concept of thermal spike is contentious but has been

supported by molecular dynamic simulations.[44–46] In context of the thermal spike, the pronounced effect of deposition temperature is rather surprising as it is difficult, at first sight, to understand how the substrate temperature of this order is significant when energies well in excess of $10^4$ K occur in the thermal spike. Below, we offer a preliminary description which shows that the effect of deposition temperature may be significant in the later stages of the thermal spike. Using the thermal spike model of relaxation, the incremental increase in density can be expressed as:

$$\frac{\Delta\rho}{\rho}=\frac{f}{1-f+\beta}, \tag{2}$$

where $f$ is the ion penetration probability and $\beta$ is the number of atomic hops per incident ion. Most analytic models assume that the thermal spike starts as a delta function at a single site with an effective temperature equivalent to the ion energy, and that the energy is dissipated by thermal diffusion.[42] The temperature distribution in a thermal spike from an ion of energy $E$ at position $r$ after time $t$ is

$$T(r,t)=\frac{E}{c(4\pi Dt)^{3/2}}\exp\left(-\frac{r}{4Dt^2}\right), \tag{3}$$

where $c$ is the thermal capacity and $D$ the thermal diffusivity. The increase in temperature causes thermally activated diffusion so that the total number of atomic hops in one spike is given by

$$\beta=\int_{r_1}^{\infty}4\pi r^2 dr\int_{t_1}^{\infty}n_0\nu_0\exp\left(-\frac{E_0}{kT(t,r)}\right)dt, \tag{4}$$

where $n_0$ is the atomic density defined as $(\frac{4}{3}\pi a^3)^{-1}$, $\nu_0$ the phonon frequency, and $E_0$ the activation energy for atomic diffusion. It is convenient to express Eq. (4) in atomic units by taking the heat capacity to be $3k$, so $c=9k/4\pi a^3$ and $D=\nu_0 a^2$. Expressing $r'=r/a$, $t'=t/\nu_0$, then integrating over $t'$ and using the reduced temperature, $\tau=kT/E_0$, gives

$$\beta=\int_{\tau_1}^{\tau_2}\tau^{-8/3}\exp\left(-\frac{1}{\tau}\right)d\tau \tag{5}$$

so the total number of hops within the limits $\tau_1\rightarrow 0$ and $\tau_2\rightarrow\infty$ is

$$\beta=0.016p\left(\frac{E}{E_0}\right)^{5/3}, \tag{6}$$

where $p$ is a material parameter of order 1. This is the $\beta$ value used in Eq. (2) thus far. The main contribution to $\beta$ can be found from

$$\frac{d\beta}{d\tau}=\tau^{-8/3}\exp\left(-\frac{1}{\tau}\right). \tag{7}$$

Equation (7) is plotted in Fig. 9 which shows that the majority of the hops occur when the reduced temperature at the spike center is $\tau\approx\frac{3}{8}$, or about $10^4$ K for $E_0=3$ eV, not at the very high temperature in the initial stages of a spike. Therefore, the deposition temperature will be significant when it is a substantial part of $E_0$ rather than of $E$. Indeed, some recent molecular dynamic simulations suggest that the spike starts with a finite size and relatively low temperature.[44–47] Thus, the deposition temperature is now a significant fraction of the spike temperature, explaining, at least qualitatively, why the low substrate temperature affects the relaxation rate. Although Eq. (4) does not give a quantitative description of the temperature dependence, it does account for the decrease in $T_1$ with ion energy. A decrease in $T_1$ with ion energy is consistent with thermally activated process during a thermal spike, with higher energies leading to further relaxation.

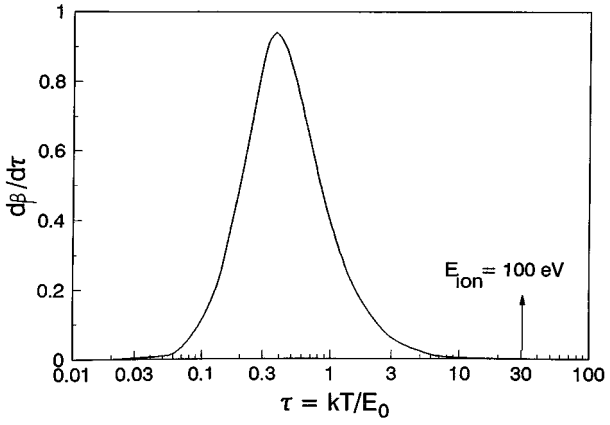


FIG. 9. Graphical representation of Eq. (8) from the text, showing that majority of atomic hops in one thermal spike due to temperature elevation occur around $10^4$ K.

## V. CONCLUSIONS

The variation of the optical band gap and electronic properties of carbon films deposited using a FCVA was studied as a function of the ion energy. The optical gap is correlated to the $sp^3$ fraction, reaching a maximum of 2.3 eV at 85%, and varies linearly with the $sp^2$ fraction. The bulk electronic and optical properties of *ta*-C are shown to be controlled by the residual $sp^2$ fraction, even when the $sp^3$ ''diamondlike'' content is as high as 85%. Furthermore, the observed decrease in ESR linewidth with increasing ion energy is consistent with an increase is $sp^2$ cluster size over which defect states are localized. The effect of deposition temperature on film properties at two ion energies was also reported. The properties were found to sharply change with substrate temperature. The temperature at which the transition from *ta*-C to *a*-C occurs is ≈200 °C for 90 eV ions which decreased to ≈140 °C when the ion energy was increased to 130 eV. The electronic and optical properties however do not show any sharp transition, which is consistent with these properties always being controlled by the $sp^2$ bonded carbon component. The gradual change in the electronic properties with $T_s$ suggests that ordering of the $sp^2$ sites starts to occur well below the transition temperature. The transition of *ta*-C to *a*-C with deposition temperature is attributed to the diffusion of subplanted atoms to the surface via activated thermal diffusion, leading to the relaxation of stress and quenched-in density increase. A preliminary description of the temperature dependence is offered in context of the subplantation model, however a detailed model is lacking.

## ACKNOWLEDGMENTS

The authors would like to thank S. Sattel and B. Kleinsorge for PDS measurements. We would also like to thank Professor R. L. Boxman and Dr. Y. Yin for helpful discussions on the temperature results. M. C. wishes to acknowledge the financial support from Multi-Arc Inc.

[1] J. Robertson, Prog. Solid State Chem. **21**, 199 (1991); Surf. Coat. Technol. **50**, 185 (1992).
[2] J. Robertson, Philos. Trans. R. Soc. London, Ser. A **342**, 277 (1993).
[3] Y. Lifshitz, S. R. Kasi, and J. W. Rabalais, Phys. Rev. Lett. **68**, 620 (1989).
[4] Y. Lifshitz, S. R. Kasi, J. W. Rabalais, and W. Eckstein, Phys. Rev. B **41**, 10468 (1990).
[5] D. L. Pappas, K. L. Saenger, J. Brueley, W. Krakow, J. J. Cuomo, T. Gu, and R. W. Collins, Appl. Phys. Lett. **67**, 984 (1995).
[6] F. Xiong, Y. Y. Chang, and R. P. H. Chang, Phys. Rev. B **48**, 8016 (1993).
[7] A. A. Voevodin, S. J. P. Laube, S. W. Walck, J. S. Solomon, M. S. Donley, and J. S. Zabinski, J. Appl. Phys. **78**, 4123 (1995).
[8] I. I. Aksenov, S. I. Vakula, V. G. Padalka, R. E. Strelnitski, and V. M. Khoroshikh, Sov. Phys. Solid State **25**, 1164 (1980).
[9] D. R. McKenzie, D. Muller, and B. A. Pailthorpe, Phys. Rev. Lett. **67**, 773 (1991).
[10] P. J. Fallon, V. S. Veerasamy, C. A. Davis, J. Robertson, G. A. J. Amaratunga, W. I. Milne, and J. Koskinen, Phys. Rev. B **48**, 4777 (1993).
[11] B. F. Coll and M. Chhowalla, Surf. Coat. Technol. **79**, 76 (1996).
[12] R. Lossy, D. L. Pappas, P. A. Roy, J. J. Cuomo, and V. M. Sura, Appl. Phys. Lett. **61**, 171 (1992).
[13] S. Falabella, D. B. Boercker, and D. M. Saunders, Thin Solid Films **209**, 165 (1992).
[14] A. Anders, S. Anders, I. G. Brown, M. R. Dickinson, and R. A. MacGill, J. Vac. Sci. Technol. B **12**, 815 (1994).
[15] H. J. Scheibe and B. Shultrich, Thin Solid Films **246**, 92 (1994).
[16] J. Robertson and E. P. O'Reilly Phys. Rev. B **35**, 2946 (1987).
[17] J. Robertson, Diam. Relat. Mater. **4**, 297 (1995).
[18] D. A. Drabbold, P. A. Fedders, and P. Stumm, Phys. Rev. B **49**, 16415 (1994).
[19] U. Stephan, T. Frauenheim, P. Blaudeck, and G. Jungnickel Phys. Rev. B **49**, 1489 (1994).
[20] Y. Lifshitz, G. D. Lempert, and E. Grossman, Phys. Rev. Lett. **72**, 2753 (1994).
[21] Y. Lifshitz, G. D. Lempert, E. Grossman, I. Avigal, C. Uzan-Saguy, R. Kalish, J. Kulik, D. Marton, and J. W. Rabalais, Diam. Relat. Mater. **4**, 318 (1995).
[22] S. Sattel, T. Giessen, H. Roth, M. Scheib, R. Ramlenski, R. Brenn, H. Ehrhardt, and J. Robertson, Diam. Relat. Mater. **4**, 333 (1995); **5**, 425 (1996).
[23] J. Robertson, Diam. Relat. Mater. **2**, 984 (1993); **3**, 361 (1994).
[24] I. I. Aksenov, V. A. Belous, and V. G. Padalka, Sov. J. Plasma Phys. **4**, 425 (1978).
[25] M. Chhowalla, C. A. Davis, M. Weiler, B. Kleinsorge, and G. A. J. Amaratunga, J. Appl. Phys. **79**, 2237 (1996).
[26] A. S. Argon, V. Gupta, H. S. Landis, and J. A. Cornie, Mater. Sci. Eng. A **107**, 41 (1989).
[27] A. A. Plyutto, V. N. Rhyzhkov, and A. T. Kapin, Sov. Phys. JETP **20**, 328 (1965).
[28] W. D. Davis and H. C. Miller, J. Appl. Phys. **40**, 2212 (1969).
[29] M. A. Tamor, W. C. Vassell, and K. R. Carduner, Appl. Phys. Lett. **58**, 592 (1991).
[30] R. H. Jarman, G. J. Ray, and R. W. Stadley, Appl. Phys. Lett. **49**, 1065 (1986).
[31] M. Weiler, S. Sattel, T. Giessen, K. Jung, H. Ehrhardt, V. S. Veerasamy, and J. Robertson, Phys. Rev. B **53**, 1594 (1996).
[32] R. A. Street, *Hydrogenated Amorphous Silicon* (Cambridge University Press, Cambridge, 1991).
[33] B. Meyerson, and F. W. Smith, J. Non-Cryst. Solids **35**, 435 (1979).
[34] V. S. Veerasamy, G. A. J. Amaratunga, J. S. Park, H. S. Mackenzie, and W. I. Milne, IEEE Trans. Electron Devices **42**, 577 (1995).
[35] V. S. Veerasamy, J. Yuan, G. A. J. Amaratunga, W. I. Milne, K. W. R. Gilkes, and L. M. Brown, Phys. Rev. B **48**, 17954 (1993).
[36] F. J. Clough, B. Kleinsorge, W. I. Milne, J. Robertson, G. A. J. Amaratunga, and R. Roy, Electron. Lett. **32**, 498 (1996).
[37] G. A. J. Amaratunga, J. Robertson, V. S. Veerasamy, W. I. Milne, and D. R. McKenzie, Diam. Relat. Mater. **4**, 635 (1995).
[38] M. Hoinkis, E. D. Tober, R. L. White, and M. S. Crowder, Appl. Phys. Lett. **61**, 4729 (1989).
[39] S. Schutte, S. Will, H. Mell, and W. Fuhs, Diam. Relat. Mater. **2**, 1360 (1993).
[40] A. Sakadi, Y. Bounouh, M. L. Theye, J. von Bardeleben, J. Cernogora, and J. L. Favre, Diam. Relat. Mater. **5**, 434 (1996).
[41] C. A. Davis, Thin Solid Films **226**, 30 (1993).
[42] F. Seitz and J. S. Kohler, *Solid State Physics*, edited by F. Seitz (Academic, New York, 1956), Vol. 2, p. 256.
[43] D. G. McCulloch, E. G. Gerstner, D. R. McKenzie, S. Prawer, and R. Kalish, Phys. Rev. B **52**, 850 (1995).
[44] T. Diaz de la Rubia, R. S. Averback, R. Benedek, and W. E. King, Phys. Rev. Lett. **59**, 1930 (1987).
[45] M. Ghaly and R. S. Averback, Phys. Rev. Lett. **72**, 364 (1994); Nucl. Instrum. Methods Phys. Res. B **90**, 191 (1995).
[46] T. Diaz de la Rubia and G. H. Gilmer, Phys. Rev. Lett. **74**, 2507 (1995).
[47] T. Diaz de la Rubia, Mater. Res. Soc. Symp. Proc. **373**, 555 (1995).